



HAL
open science

Non-aromatic carbonaceous species formed in the circumstellar innerlayers of evolved stars

Lidia Martínez, Gonzalo Santoro, Pablo Merino, Mario Accolla, Koen Lauwaet, Jesús Sobrado, Hassan Sabbah, Ramón J Pelaez, Victor J Herrero, Isabel Tanarro, et al.

► **To cite this version:**

Lidia Martínez, Gonzalo Santoro, Pablo Merino, Mario Accolla, Koen Lauwaet, et al.. Non-aromatic carbonaceous species formed in the circumstellar innerlayers of evolved stars. *Nature Astronomy*, 2020, 4 (1), pp.97-105. 10.1038/s41550-019-0899-4 . hal-03085475

HAL Id: hal-03085475

<https://hal.science/hal-03085475>

Submitted on 21 Dec 2020

HAL is a multi-disciplinary open access archive for the deposit and dissemination of scientific research documents, whether they are published or not. The documents may come from teaching and research institutions in France or abroad, or from public or private research centers.

L'archive ouverte pluridisciplinaire **HAL**, est destinée au dépôt et à la diffusion de documents scientifiques de niveau recherche, publiés ou non, émanant des établissements d'enseignement et de recherche français ou étrangers, des laboratoires publics ou privés.

Non-aromatic carbonaceous species formed in the circumstellar inner-layers of evolved stars

Lidia Martínez¹⁺, Gonzalo Santoro¹⁺, Pablo Merino^{1,2+}, Mario Accolla¹, Koen Lauwaet³, Jesús Sobrado⁴, Hassan Sabbah⁵, Ramón J. Pelaez⁶, Victor J. Herrero⁶, Isabel Tanarro⁶, Marcelino Agúndez², Alberto Martín-Jimenez³, Roberto Otero³, Gary J. Ellis⁷, Christine Joblin^{5*}, José Cernicharo^{2*} and José A. Martín-Gago^{1*}

¹Instituto de Ciencia de Materiales de Madrid (ICMM-CSIC). Materials Science Factory. Structure of Nanoscopic Systems Group. C/ Sor Juana Inés de la Cruz 3, 28049 Cantoblanco, Madrid, Spain.

²Instituto de Física Fundamental (IFF-CSIC). Group of Molecular Astrophysics, C/ Serrano 123, 28006 Madrid, Spain

³IMDEA Nanociencia, Ciudad Universitaria de Cantoblanco, 28049 Cantoblanco, Madrid, Spain

⁴Centro de Astrobiología (CAB, INTA-CSIC). Crta- de Torrejon a Ajalvir km4, 28850, Torrejon de Ardoz, Madrid, Spain.

⁵IRAP, Université de Toulouse, CNRS, CNES, 9 Av. du Colonel Roche, 31028 Toulouse Cedex 4, France

⁶Instituto de Estructura de la Materia (IEM-CSIC). Molecular Physics Department. C/Serrano 123, 28006 Madrid, Spain.

⁷Instituto de Ciencia y Tecnología de Polímeros (ICTP-CSIC). C/ Juan de la Cierva 3, 28006-Madrid, Spain.

+ Equally contributed

*Corresponding authors: gago@icmm.csic.es, jose.cernicharo@csic.es, christine.joblin@irap.omp.eu

Abstract.

Evolved stars are a foundry of chemical complexity, gas and dust that contribute to the formation of the building blocks of planets and life. Nucleation of dust takes place first at the photosphere of evolved stars. Despite their importance, these cosmic regions remain hidden to many observations and dust formation processes are still poorly understood. Laboratory astrophysics provides a complementary route to unveil these chemical processes but the majority of experiments are based on combustion or plasma decomposition of molecular precursors in physical conditions far removed from those in space. We have built an unprecedented ultra-high vacuum machine combining atomic gas aggregation with advanced *in-situ* characterization techniques to reproduce and characterize the bottom-up dust formation process. We show that carbonaceous dust analogues formed from low-pressure gas-phase condensation of C atoms in a hydrogen atmosphere in a C/H₂ ratio similar to that reported for evolved stars leads to the formation of amorphous C nanograins, and C-clusters aliphatic in nature. Aromatic species or fullerenes are not effectively formed under these physical conditions.

Stars, like our Sun, in their final stages of evolution reach the asymptotic giant branch (AGB) accompanied by a massive ejection of matter containing the vast chemical complexity that provides the building blocks of planets and the main ingredients necessary for the emergence of life¹⁻³. The advent of powerful radio-telescopes like ALMA, with improved radial resolution and sensitivity, opens the possibility to outline the basic physical and chemical conditions in which stardust is formed in the circumstellar envelopes (CSE)⁴⁻⁶. This dust, which consists of silicates or carbonaceous material depending on the C/O elemental abundance ratio of the AGB star, will then be ejected into the interstellar medium (ISM) where, after processing, it becomes involved in the formation of new stars and planets. However, the chemical nature of the dust seeds and carbonaceous molecules produced by C-rich evolved stars, as well as the chemical routes leading to them, is still controversial. The dust seeds are first generated in the vicinity of the photosphere, at about 1-2 stellar radii⁷. In these regions, carbon nucleates into nanometer-sized grains in an equilibrium process with a low degree of ionization due to the absence of energetic radiation. The nucleation zone of an AGB star can be regarded as a homogeneous dense atomic cloud in the photosphere of the star which, contrary to the outer layers, is devoid of UV photons. Physical parameters in nucleation zones remain uncertain because they are difficult to derive from observations⁴. Moreover, there is a lack of experiments able to approach the relevant physical conditions, since most rely on energetic plasmas, combustion or decomposition of molecular precursors under conditions very unlike those in the dust formation regions of CSE⁸. Therefore, understanding the formation and nature of carbon stardust is complex and cannot be addressed solely by astronomical observations; dedicated laboratory simulations are required⁹⁻¹⁵.

A related issue is the formation of large carbonaceous molecules, polycyclic aromatic hydrocarbons (PAHs) and fullerenes. PAHs, identified by the emission of aromatic infrared bands (AIBs)¹⁶, are widespread in regions of massive star formation and in C-rich protoplanetary and planetary nebulae. Buckminsterfullerene C₆₀ has been detected in some of these environments^{6,17,18} and its cation is also present in the diffuse ISM¹⁹. A robust explanation of how these large molecules form is still lacking, especially in evolved stars where AIBs are only detected at late stages when the star evolves from red giant to white dwarf emitting ultraviolet (UV) radiation²⁰.

In this work, using an unprecedented ultra-high vacuum (UHV) experimental setup²¹ we investigate the basic carbonaceous chemistry taking place in the dust formation region of CSEs. Unlike previous experiments, our approach produces carbon dust seeds using exclusively gas-phase C atoms and molecular hydrogen in a ratio close to that in the atmospheres of AGB stars without the requirement for introducing *ad hoc* C-bearing molecular precursors, such as acetylene or methane. Under these conditions, we show that carbon nanosized-particles, pure carbon clusters and carbon species of aliphatic nature are efficiently formed, whereas aromatics are only present at trace levels and no fullerenes are detected. Our results reproduce the relative abundances of simple molecules detected in CSEs, such as C₂H₂ and C₂H₄, which are directly generated by bottom-up chemistry and are simulated by a simple chemical kinetics model. Our data suggest that the pressures in circumstellar condensation environments are not sufficiently high for initiating cyclization mechanisms²² and the formation of aromatic species must occur via other processes. We suggest that one pathway could be through thermal processing of aliphatic material on the surface of dust.

RESULTS

Ultra-high vacuum Gas Aggregation Sources for mimicking the Dust Formation Region of CSEs.

Our experimental set-up, called *Stardust*²¹, is an UHV machine specifically conceived to simulate in the laboratory the complex conditions of star-dust formation and processing in the environment of evolved stars. *Stardust* comprises six interconnected UHV modules, offering a high level of control over both the fabrication and processing of cosmic dust analogues. In addition, a collection of *in situ* characterization techniques are available. UHV technology is mandatory because of the high reactivity expected of the formed carbon nanostructures to atmospheric and residual gases²³. A more detailed technical description is given in Supplementary Information 1.

Many different techniques have been proposed to form dust analogues, all with their own limitations and advantages. In Supplementary table 1 we present a detailed critical compilation of the most commonly used techniques. Among them, laser ablation is one of the best suited ones¹⁰ which has been used, for instance, to simulate the reformation mechanisms of cosmic grains taking place at low temperature directly in the ISM¹⁵. In *Stardust*, we have chosen a sputter gas aggregation source (SGAS) because it is able to generate small clusters nano-sized particles by gas-phase aggregation of individual atoms in a weakly ionized environment²⁴. Gas temperature during aggregation can be estimated to be lower than 1000 K²⁴, in the range of the condensation temperatures of solids in CSEs (500-2000 K)^{7,25}. Thus, the chemistry proceeds via atom aggregation under conditions in which most of the reactions that occur are neutral-neutral, bimolecular and termolecular, closely resembling what happens in the dust formation region of CSEs.

The working principle of our experiment is the vaporization of C atoms from a graphite target, using Ar as the sputtering gas. Usually, standard growth methods that employ physical vapor deposition or magnetron sputtering produce nanoparticles or grains directly on the substrate as result of surface diffusion of the adsorbed atoms^{26,27}. In the case of the SGAS, nanoparticles and clusters form from gas phase reactions as the sputtered material gets trapped in the aggregation zone of the machine.

In this work we unveil the formation of carbonaceous dust grains starting with a gas mixture containing the two most relevant species: carbon and molecular hydrogen. In carbon-rich CSEs oxygen is locked into CO and SiO and therefore is not available to form dust^{28,29}. Fig. 1 shows a pictorial representation of a CSE where typical carbon and hydrogen densities are provided. Supplementary table 2 further compares the conditions achieved during the experiments in the gas aggregation zone with those in the dust formation zone of CSEs. A scheme of *Stardust* in the configuration used for these experiments is shown in Fig. 1. The experiments start with the vaporization of C atoms, followed by the injection of H₂. The vaporized C atoms react with H₂ and are subsequently dragged through a nozzle by differential pressure into the next chambers, where they are either analysed in gas phase or collected on inert surfaces for further analysis. In our experiments, we have used different chemically-inert substrates to collect the carbonaceous stardust analogues for further studies, including Au, SiO₂ or highly oriented pyrolytic graphite (HOPG). The results we show hereafter are unaffected by the chosen substrate. Once the formed species pass the nozzle of the first chamber, no further growth takes

place in the expansion. The composition of the small gas-phase species is analysed *in situ* by mass spectrometry (MS) and Optical emission spectroscopy (OES). The material generated can be collected on a surface at position “SAMPLE-1” for *ex situ* studies, such as laser desorption ionization (LDI) mass spectrometry or Atomic Force Microscopy (AFM). Finally, the deposit (at position Sample 2 in Fig.1) is characterized *in situ* in a third chamber by Thermal Programmed Desorption (TPD).

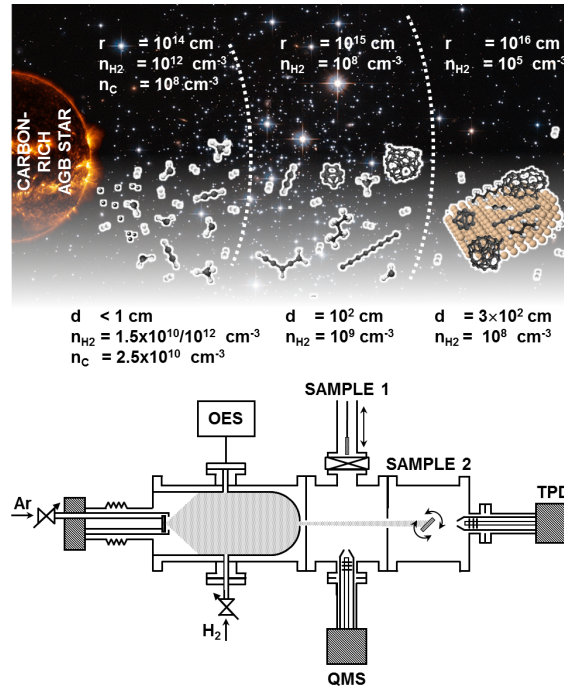


Fig. 1 | Production of stardust analogues. Upper part: pictorial representation of the CSE of a C rich AGB star, where typical carbon and hydrogen densities at given distances are provided following reference²⁸. **Lower part:** Schematic of the Stardust machine configuration used in these experiments, with typical C and H₂ densities considered. From left to right: there are three different vacuum environments: aggregation zone, where OES measurements are performed and H₂ introduced; expansion area, where the quadrupole mass spectrometer (QMS) is placed and we collect samples for *ex situ* studies (sample 1 position), and analysis area (sample 2), where thermal programmed desorption (TPD) is performed.

The initial gas-phase vaporized C atoms may interact with residual or injected molecular hydrogen at different densities, and there are no other species involved except Ar (the residual density before magnetron operation, excluding Ar and H₂, is about 10⁷ cm⁻³). The vaporized C atoms have a density of about 2.5x10¹⁰ atoms·cm⁻³ as estimated from the sputtering energy (200 eV), the total drag current (200 mA) and the yield of emitted C atoms per impinging Ar⁺ ion³⁰. Under these conditions, sputtering of C atoms is preferential than C₂ and C₃ using Ar⁺³¹. Although the estimated value is some orders of magnitude higher than that accepted for the dust nucleation zone of stars²⁸, it provides an effective method to accelerate the chemistry, which takes years in a real AGB envelope. Setting higher C densities together with an Ar overpressure, which accelerates the number of three-body reactions, are the two strategies adopted to overcome the exposure time limitation. Regarding the hydrogen, two cases are considered: low and high densities. In the first case, H₂ molecules and C atoms are in the same proportion, which

can be achieved either using residual hydrogen or by introducing very low H_2 densities that are estimated in the range of $1.5 \times 10^{10} \text{ mol}\cdot\text{cm}^{-3}$, a value typically accepted for the dust nucleation zone at distances from the star of 2-3 R^* ²⁸. In the second case, a high H_2 density is achieved by introducing extra hydrogen at a concentration estimated at $1.5 \times 10^{12} \text{ mol}\cdot\text{cm}^{-3}$, two orders of magnitude higher than that of vaporized C atoms. This situation provides a more appropriate concentration to simulate the chemistry in CSE in terms of H_2/C abundance (≈ 1000)³².

Structure of the carbonaceous stardust analogues produced. Fig. 2a-b shows typical AFM images obtained on the C-dust collected on a SiO_x surface at the position labelled “SAMPLE 1” in Fig. 1. Two different morphological features can be identified. Firstly, carbonaceous nanosized grains (encircled in white in Fig. 2a) are efficiently produced as the most abundant constituents^{10,15}, with a surface density that increases with deposition time. These spherical grains exhibit an extremely narrow size distribution with an average size of 9 nm, and each is comprised of more than 10^5 C atoms (see Fig. 1a inset). Although larger grains (typically 100 nm) are thought to be present in space, in *Stardust* the nanoparticle size is conditioned by the geometry and experimental parameters and can be considered to represent the initial stages of carbonaceous dust growth. While the images of Fig. 2 were recorded for the case of low hydrogen concentration, similar structures can be found for the high H_2 concentrations.

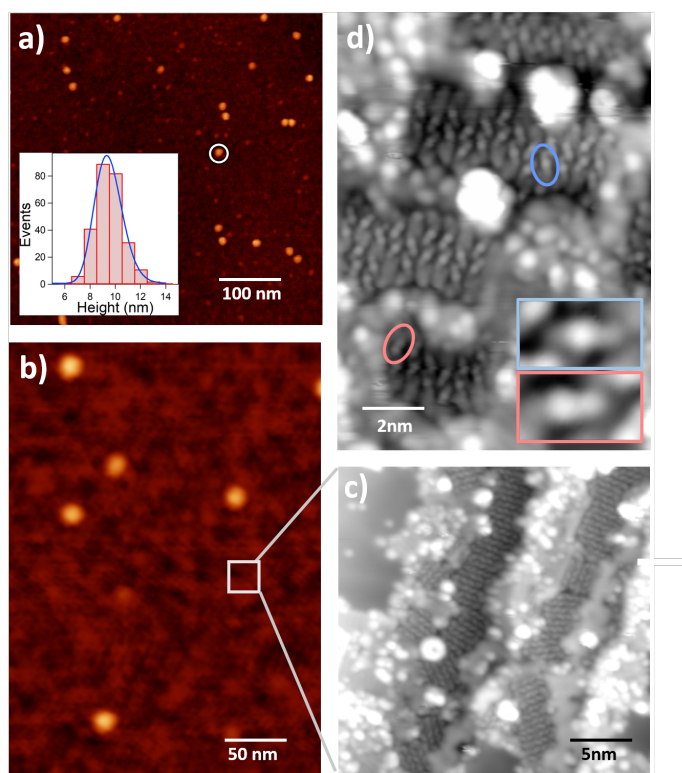


Fig. 2 | Production and structure of the stardust analogues. a-b, AFM images recorded *ex situ* showing the presence of C-nanoparticles and small clusters forming an almost continuous layer. A single nanoparticle is encircled in fig. 2a. Inset of fig. 2a shows the size distribution in a bar-histogram performed over several images. The blue line represents the log-normal fitting of the size distribution c-d, *in situ* recorded STM images of a C-cluster film deposited on a Au surface. Scanned area: $25 \times 25 \text{ nm}^2$, recorded at

50 pA, 1400 mV. Inset: Zoom of the rectangular area 5x3 nm², I= 10 pA, V=1400 mV. Two small molecules are encircled and zoomed in the inset of fig. 2d. The white lines showing the enlarged area in fig. 2b are for clarity and do not correspond to the exact area where measurements were taken. All images were recorded for the case of low-hydrogen concentration.

Besides the carbonaceous nanograins, the other principal constituent of the C-dust analogues can be observed on the “flat” regions of Fig. 2b, where a thin mantle of material is observed, for instance in the area marked by a white square (see Supplementary Information 3). Structural resolution of these zones cannot be achieved using standard AFM, and more powerful *in situ* microscopies are required. Fig. 2c-d shows a scanning tunnelling microscope (STM) images obtained from the C analogues deposited on a Au surface. A STM-based detailed characterization of the carbon products obtained with the SGAS is complicated due to the large number of different species generated during the experiment and their sub-nanometric size. However, the capabilities of low temperature LT-STM allow us to resolve individual clusters in real-space with Å-scale resolution. At room temperature (300K) molecular clusters diffuse on the surface with high speed impeding their rigorous identification. At low temperatures (4K) the adsorbed products remain immobilized on the surface.

Fig. 2c shows a wide plethora of individual nanometer-sized structures at the surface, with apparent heights ranging from 1 to 5 Å that correspond to small amorphous C-clusters, but are difficult to ascribe to a particular cluster type due to the varying shapes. Some of these small molecules can self-assemble on the surface forming 2D ordered islands (see Fig. 2d). This process is surface-mediated suggesting electrostatic interactions between the molecules upon adsorption on surfaces. The structures forming the ordered regions are no longer than 8 Å and with a maximum apparent height of 0.6 Å (see inset). The small size suggests that they correspond to individual molecules of only 3 to 5 C atoms. Unambiguous assignment to a precise chemical structure is difficult due to the fact that STM images show a topography that is convoluted with the electronic structure of the inspected element.

Aliphatic nature of the dust analogues. To further understand the nature of these carbon analogues we used gas-phase analysis techniques. The Swan C₂ lines observed by OES are observed in Fig. 3a in the presence of low H₂ density, but are not found in the case of higher H₂ density. On the contrary, the H_α emission line is only observed at high H₂ density. These observations suggest that excited H atoms are generated during the chemical evolution, involving C₂ + H₂ → CCH + H. The absence of the C₂ lines at high H₂ density indicates that most of the excited C₂ formed is consumed in this reaction. Interestingly, C₂ and H species are only detected in the regions close to the magnetron, which compares very well to observations from the photosphere of evolved stars where atomic hydrogen has been found and C₂ bands are prominent³³. See supplementary information 4 for complete OES spectra.

Fig. 3b presents the evolution of the masses of some relevant species during the experiment recorded at position QMS of Fig. 1b. The ON region in the figure corresponds to the period where the magnetron is switched on, before and after this point we obtain the background values. Unfortunately, for these low masses a direct assignment with their parent molecule is not

straightforward due to the electron ionization of the quadrupole that induces cracking patterns. Nevertheless, we discuss the most important contribution for every mass. The most striking change for the case of high H_2 densities is the predominant formation of mass 26 amu, which mainly corresponds to C_2H_2 along with fragments of C_2H_4 , C_2H_6 and larger aliphatic molecules. An increase of mass 16 amu is also observed, corresponding to methane. In the case of high H_2 densities the formation of these species are more abundant and we also detect an increase in the main ionization fragments of ethane (C_2H_6), ethylene (C_2H_4), propane (C_3H_8) and larger alkanes (which contribute to most of the masses). Importantly, here these species were formed directly from C atoms and molecular hydrogen, without introducing them as precursors, and using ratios and aggregation processes similar to those reported to take place in the dust formation zone of CSEs¹⁴. Fig. 3b shows a decrease in the partial pressure of H_2 when C evaporation is initiated, suggesting that H_2 is partially consumed by chemical reactions that occur in the aggregation zone. It is important to remark that neither benzene (78 amu) nor toluene (91 amu) are detected, indicating that they are below the detection limit (3×10^3 mol cm^{-3}). Interestingly, masses 18 and 32, corresponding to water and oxygen respectively, are unchanged with respect to their background pressure, indicating that, although present as residual gases, they are not taking place in the reactions.

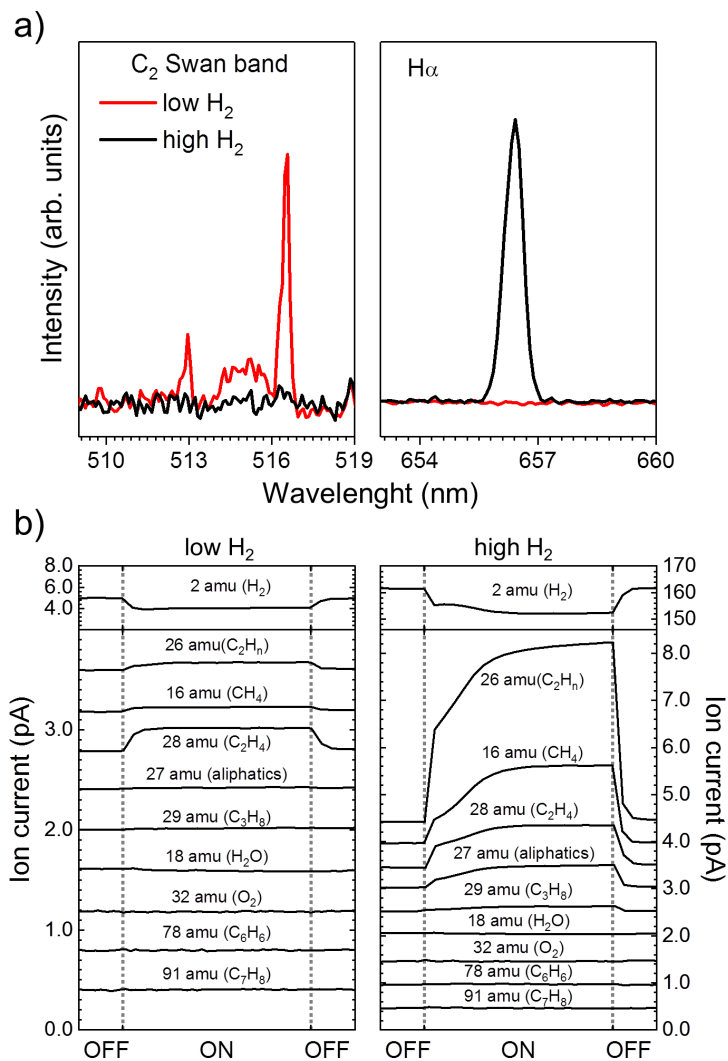


Fig. 3 | Spectroscopic characterization of the molecular species. **a**, Optical emission spectra recorded at position OES in Fig. 1b for low and high H₂ densities. **b**, In situ gas-phase mass spectroscopy detection at position QMS of most important masses for low and high H₂ densities. Vertical dashed lines indicate the time period where the magnetron was switched on and off. All masses have been offset for clarity.

We have performed *ex situ* laser desorption ionization mass-spectrometry (LDI-MS) in the so-called AROMA set-up³⁴, a machine with high sensitivity for PAH detection. Fig. 4 provides the ion distribution obtained by desorption/ionization of representative samples grown with both H₂ densities, showing that the molecular species generated have < 20 carbon atoms. C-clusters with a low degree of hydrogenation are observed for species containing 4 to 9 C atoms. Pure carbon clusters are observed from C₈⁺ to C₁₉⁺, and above C₉⁺ these are poorly hydrogenated, which can be understood by the formation of ring structures with lower reactivity³⁵. Above 300 amu the signal completely vanishes, indicating the absence of fullerenes, particularly C₆₀ (see Supplementary Figure 4 for full mass range spectra).

The results from LDI-MS are summarized in the insets of Fig. 4 where the species generated are classified in families (see Supplementary Information 5 and methods). The analysis suggests a higher abundance of C_nH_m clusters for low H₂ density, indicating the formation of more saturated aliphatic species at higher H₂ density, which are not found by LDI-MS but evidenced by QMS (Fig. 3). Benzene or toluene, as key aromatic species, are marginally detected either in LDI-MS or in the QMS measurements. In LDI-MS, a few aromatic species are evidenced in very low abundance (total of 3% for both H₂ densities), the largest one being C₁₆H₁₀ (Fig. 4). Therefore, it appears that the chemistry involved in the CSE does not favour the formation of PAHs, whose abundance can reach up to 18% of the total carbon species in the ISM³⁶. Fig. 4 shows that low masses, as C₂H₂, are more importantly detected for the case of low H₂ density. However, this quantification shall not be considered as they correspond to volatile species that remain included in the clusters and their total abundance may change from one sample to another.

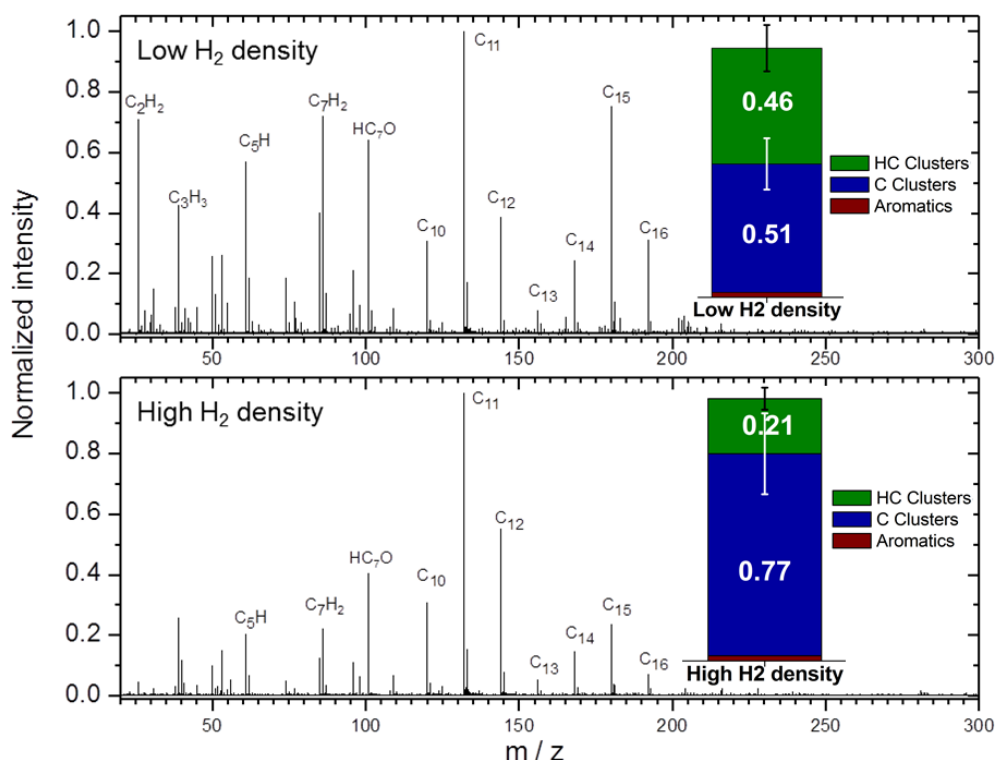


Fig. 4 | Ex situ laser desorption/ionization mass spectrometry (LDI-MS) from samples grown with a low (upper panel) and high (lower panel) H₂ densities. Data are normalized to the highest peak. Insets: Stacked bar graphs summarizing the family compositions by double bond equivalent (DBE) analysis on the full spectra (see Methods). The error bars correspond to the relative standard deviation obtained for the total ion signal over a mass range for each family of compounds.

DISCUSSION

Kinetic and energetic modelling. Considering the QMS and LDI-MS results we have constructed a time-dependent chemical kinetics model that computes the evolution of the chemical composition of a gas mixture. The model follows the formation of carbon-containing molecules from the precursor C + H₂. That is, we aim to predict the main molecules that can be formed and to understand which are the underlying chemical reactions behind their formation.

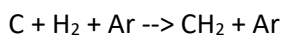
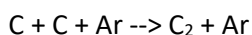
We use a gas-phase chemical network consisting of about 100 neutral and ionic pure carbon clusters and hydrocarbons containing up to 10 carbon atoms. These species are linked by about 2000 chemical reactions, whose rate constants are extracted from the literature on combustion chemistry, atmospheric chemistry, astrochemistry, as well as from specific chemical kinetics studies³⁷.

The initial conditions correspond to those at the gas aggregation zone in the high H₂ dose experiment (see first section). The starting composition of the gas consists of a mixture of Ar/Ar⁺/H₂/H/C with mole fractions 1.0/10⁻⁴/1.6x10⁻⁶/10⁻⁷/2.6x10⁻⁸. We consider that the gas is trapped in the aggregation zone at a constant pressure of 66 mbar (measured value) and a constant temperature of 500 K, which could be considered as an averaged representative value. In a second stage, the gas is neutralized and expands reaching a pressure of 0.1 mbar and a

temperature of 300 K at a distance of 10 cm from the magnetron sources. At this stage, the sharp decrease in pressure makes the chemical reactions too slow in comparison with the dynamic time scale associated with the gas expansion, and the chemical composition remains quenched. Therefore, molecular synthesis takes place only during the first stage in the aggregation zone.

In Fig. 5 we show the results of the calculations for some relevant species. It is seen that after several tens of seconds, atomic carbon starts to be processed into different carbon-containing molecules. Pure carbon clusters such as C_3 , unsaturated hydrocarbons like C_2H_2 and C_3H_2 , and saturated hydrocarbons such as CH_4 , C_2H_6 , and C_3H_8 are abundantly formed. These results are qualitatively in agreement with the molecules detected in gas-phase (Fig. 3) in the *Stardust* machine, which indicates the disappearance of C_2 , together with the emergence of CH_4 and C_2H_2 . According to the model, the molecular synthesis takes place in various steps.

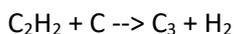
The initial step, in which carbon is transformed from atoms to molecules, proceeds via three-body reactions with Ar as third body. In particular,



are key the reactions that constitute a bottleneck to the whole process of formation of C-containing molecules. For the pressure and temperature of the model, the time scale of these reactions is of the order of tens of seconds. The bimolecular reaction of atomic carbon with H_2 to produce $CH + H$ is endothermic by about 100 kJ/mol and thus is not efficient at a temperature of 500 K.

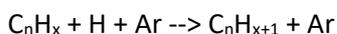
Once the above starting reactions have formed the first molecular species, the growth of molecules is driven by bimolecular reactions and three-body reactions involving neutral species. Routes involving ions are less efficient in our experimental conditions. Moreover, reactions of hydrocarbons with Ar^+ are fast and result in fragmentation³⁸, so that these reactions tend to produce a delay in the molecular synthesis.

According to the model, carbon growth mainly occurs by reactions of insertion of carbon atoms. For example, the reaction

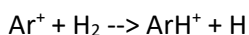


is fast³⁹ and drives the transformation from species with two carbon atoms to molecules with three C atoms. Analogous reactions of polyacetylenes with atomic carbon allow the progressive processing of carbon into aliphatic hydrocarbons of increasing complexity.

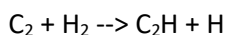
Apart from the increase of the number of carbon atoms, hydrogenation is also an important part of the chemical processing that takes place in the *Stardust* experiment. Hydrogenation essentially occurs via three-body reactions involving H atoms of the type



in which H atoms are successively added. This way, CH_4 is formed from CH_2 , and C_3H_8 from less hydrogenated species like C_3 and C_3H . Under our experimental conditions, H atoms are abundantly formed through various reactions involving ions like



There are some hydrogenation steps that mostly follow bimolecular reactions involving H_2 rather than three-body reactions involving H atoms. This is the case of the conversion of C_2 into C_2H , which occurs by the reaction



which could be rapid⁴⁰ and more efficient than the three-body reaction, $\text{C}_2 + \text{H} + \text{Ar}$.

The synthesis of hydrocarbons from atomic carbon is summarized in the scheme shown in Fig. 5. The scheme of carbon growth by C insertion and hydrogenation by three-body reactions with H can be extrapolated to larger species. However, the kinetics of reactions involving larger hydrocarbons is not so well constrained and it is likely that other routes, e.g., associations of hydrocarbon fragments of different size, will also be efficient.

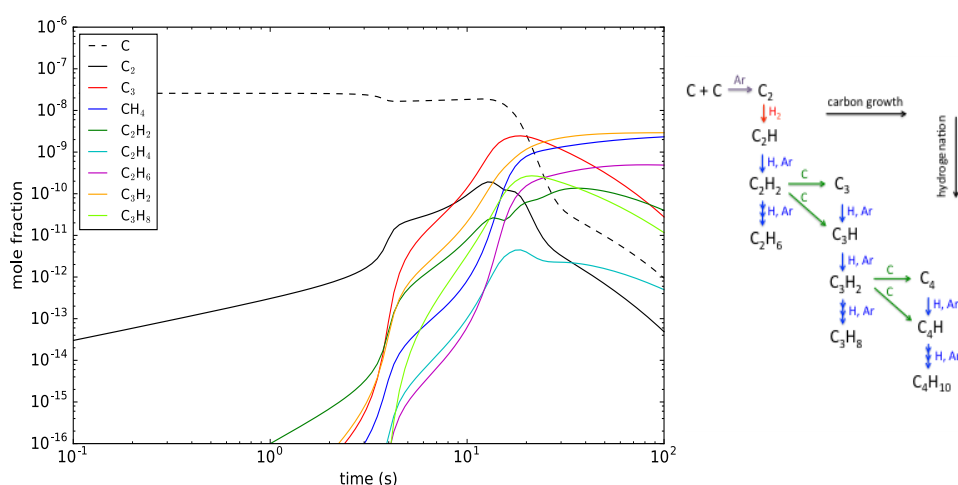


Fig. 5 | Computed evolution of the molecular species formed Left: Evolution of the chemical composition computed with the chemical kinetics model as the gas flows in the aggregation zone, calculated using the values for high hydrogen densities (see text) and at $T=500\text{K}$. Right: Chemical scheme of synthesis of hydrocarbons from atomic carbon given by the chemical kinetics model. Calculations performed for the case of high hydrogen density.

The calculations carried out at different temperatures indicate that for temperatures below 500 K (down to 300 K) the results are qualitatively similar to those obtained at 500 K, with small variation in the peak abundances. These slight deviations in abundance are caused by the dependence of the rate coefficients of the reactions involved in the molecular synthesis. At temperatures higher than 500 K the results gradually modify its behavior, with unsaturated hydrocarbons like polyacetylenic chains becoming more abundant at the expense of saturated hydrocarbons, like alkanes. At temperatures above 1000 K the model predicts that alkanes should have negligible abundances. This suggests that there could be a turning point for temperatures around 800-1000 K. Below these temperatures, hydrocarbon with high H/C ratios would form efficiently whilst at higher temperatures C-bearing molecules with low H/C ratios would dominate. This may have implications for the formation of carbonaceous material in C-rich CSEs. At thermochemical equilibrium, graphite is predicted to condense at temperatures as

high as 1500-2000 K⁴¹. However, the actual temperature at which carbonaceous dust forms in C-rich CSEs could be significantly lower because solid carbon may not be graphitic but rather in the form of less ordered materials like amorphous carbon⁴² and because the process of condensation is probably controlled by chemical kinetics rather than by thermochemical equilibrium.

Thermal induced formation of aromatics on surfaces. Fig. 6 shows a representative mass spectrum single scan at 430K from an *in situ* TPD experiment (see full TPD in Supplementary Figure 6). Although a precise assignment of masses is difficult to perform, families of C_nH_m hydrocarbons can be identified. The most abundant masses of 26 amu, 39 amu and 41 amu all belong to known fragments of larger aliphatic hydrocarbons⁴³. Interestingly, in our experiment benzene and naphthalene were observed only after annealing the deposited carbon above 355K. These aromatic species are most likely formed after a catalytic recombination of small hydrocarbons on the gold surface, a process reported in surface chemistry^{44,45}, since they were marginally (in the case of benzene) or not (in the case of naphthalene) observed in the LDI-MS analysis that is highly sensitive to aromatics. The fact that aromatics could be formed after annealing of carbonaceous aliphatics deposited on a C-rich surface needs to be further explored as a possible mechanism for the formation of these species in warm CSE environments. Indeed AIBs, the signature for PAHs, are not convincingly detected in AGBs but are observed at later stages when the star emits ultraviolet (UV) radiation that leads to photo-processing of the carbon-dust²⁰.

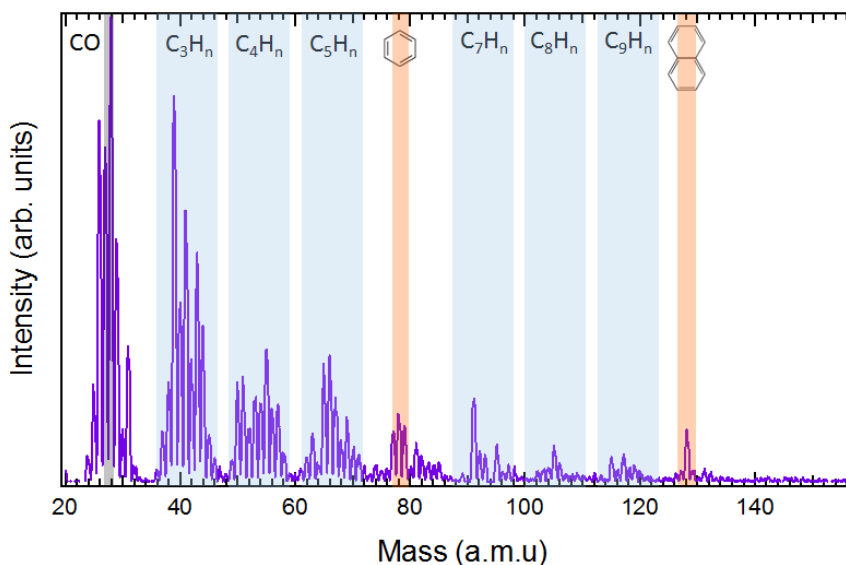


Fig. 6 | Representative mass spectrum from a thermal desorption experiment on C-analogues formed using high H_2 density on a Au surface. Temperature of 430 K.

Astrophysical implications. Carbon, nitrogen, oxygen (assumed to be in CO and SiO_x in C-rich AGBs), and hydrogen are the main actors of the molecular universe, and the combination of these elements gives rise to a plethora of organic molecules. There are several models to account for the presence

of aromatic species in the ejecta of evolved stars; one involves the polymerization of acetylene to benzene⁵ and further growth by the hydrogen abstraction acetylene addition (HACA) mechanism^{22,46}. Other scenarios involve the processing of SiC dust grains⁴⁷ or the catalytic activity of C₂H₂ on silicate surfaces⁴⁸. Although the HACA mechanism has been invoked to unravel the synthesis of PAHs in the outflows of carbon-rich AGB stars^{22,46}, our results suggest an alternative scenario. We produce acetylene in a ratio H₂/C₂H₂ of 50, compared to the 10⁴ estimated for the inner layers of AGBs⁴. This is due to the fact that we have accelerated the chemistry by introducing higher C densities. Importantly, even in these favourable conditions we do not observe an efficient formation of PAHs. Earlier models of the formation of PAHs in CSE have shown that there is a narrow temperature window, between 900 and 1100K, in which PAHs could form^{22,49}. However, the conversion of benzene to larger PAHs was found to be a bottleneck in the reaction scheme. The role of shocked regions close to the star photosphere in which temperatures higher than 1700 K could be reached have therefore been emphasized⁵⁰.

Our results also suggest the formation of a large amount of amorphous carbon nanosized grains that shall be considered the main component of the carbon stardust (see Fig. 3). Aliphatic species deposited on dust grains are susceptible to further react between themselves in a catalytically activated process leading to larger molecules or aromatic species upon thermal activation (see Fig. 6). Such a rise in temperature could be achieved in the highly UV-irradiated environments of protoplanetary nebulae where polymerization of gas species and dust chemistry could also lead to the formation of PAHs^{5,32}.

Finally, we are able to qualitatively reproduce the abundances of the C₂H₂ and C₂H₄ found in CSEs around AGB stars, indicating that SGAS, a technique not previously used in laboratory astrophysics, can be a very valuable tool to gain information on the chemistry operating in CSEs. When compared to other techniques SGASs can more closely resemble the delicate conditions of these cosmic environments (see Supplementary table 2). Most of the previously used techniques lead to the formation of aromatics, in addition to grains and clusters, either because of the use of much higher temperatures or because of the use of very high pressures of acetylene.

Conclusions

The combination of laboratory astrophysics, surface science and astronomical observations can unveil the chemical routes that operate in the inner layers of the envelope of evolved stars, providing new insights into the chemistry of carbonaceous stardust seed formation and fostering new observations. Our results suggest that PAHs might not be efficiently form during gas-phase growth in the CSE, which we show to generate aliphatic material and C-clusters together with carbonaceous nano-grains. However, the species that are deposited on dust grains are susceptible to further processing and dust can catalyse the formation of aromatic species upon thermal activation, which could take place as a result of the significant rise in dust temperature that occurs in highly UV-irradiated environments.

Methods

Fabrication of the dust analogues. The carbon dust analogues were fabricated using a scaled-up Multiple Ion Cluster Source (MICS)²¹, a type of sputtering gas aggregation source (SGAS), working under UHV conditions (base pressure 1×10^{-9} mbar) from Oxford Applied Research Ltd.. The magnetrons were loaded with a graphite target of 99.95% purity. The Ar flux used for the experiments was 150 sccm. The typical power applied to the magnetron was 100 W and the working aggregation length (distance between the magnetron and the exit nozzle) was 374 mm.

Extra-pure H₂ (99.99% purity) was injected during fabrication through one of the lateral entrances of the aggregation zone of the MICS (see Supplementary Figure 1), using gas-dosing valves with flux-regulator to inject into the UHV system. The doses used for these experiments were: 0, 4×10^{-4} and 1 sccm, with an Ar flux maintained at 150 sccm. The substrates employed for collecting the NPs are boron-doped Si(100) with its native oxide for AFM; polycrystalline Au for AROMA experiments; Au(111) and HOPG for TPD analysis.

Atomic Force Microscopy (AFM) measurements were performed in the dynamic mode using a Cervantes AFM System equipped with the *Dulcinea* electronics from Nanotec Electronica S.L. All images were analyzed using WSxM software⁵¹. AFM images were recorded *ex situ*.

Scanning tunneling microscopy (STM). Samples for scanning tunnelling microscopy (STM) were prepared in *Stardust* and transferred without exposing the samples to the atmosphere to the STM chamber, located in a different laboratory, using a UHV suitcase with an ion-getter pump (base pressure $< 1 \times 10^{-9}$ mbar) to avoid chemical reaction with environmental gases²³. This procedure can be considered as *in situ* since the surface has never been at a pressure higher than 10^{-9} mbar. Samples are deposited on an atomically flat single crystal Au(111) surface pre-cleaned by repeated sputtering/annealing cycles, which consisted of sputtering for 10 min using Ar⁺ ions at an energy of 1.25 kV and subsequent annealing at 800 K for 5 min. Clean Au(111) is later exposed to the carbon analogues for 5 minutes keeping the sample at room temperature, then immediately transferred to the UHV suitcase and to the STM chamber. The total time between sample growth and insertion in the STM cryostat was limited only by the pumping of the load lock volume. STM measurements were performed at 4K in a LT-STM (Scienta Omicron) with a base pressure $< 10^{-11}$ mbar.

Optical emission spectroscopy (OES). The light emitted by the plasma generated in front of the magnetron was collected through a fused silica window and an optical fibre of fused silica, and analysed by OES (see position in Fig. 1a) using a 193 mm focal length, motorized Czerny-Turner spectrograph (Andor, model Shamrock SR-193-i-A) equipped with a CCD camera (iDus DU420A-BVF). Two diffraction gratings with 1200 grooves/mm and 1800 grooves/mm, installed in a movable turret, provide spectral ranges of 300-1200 nm and 200-950 nm, respectively, and nominal spectral resolutions of 0.22 nm and 0.15 nm, respectively (for an input slit width of 20 μ m). The relative spectral efficiencies of all the spectroscopic equipment was quantified for both diffraction gratings with a calibrated tungsten lamp.

***In situ* mass spectrometry (MS).** The gaseous species produced during the fabrication of the C-dust analogues were detected *in situ* with a quadrupole mass spectrometer (QMS) (0-100 amu)

Prisma plus spectrometer from Pfeiffer. Lowest detectable partial pressure 10^{-10} mbar. Includes Continuous Secondary Electron Multiplier.

Laser desorption/ionization (LDI) mass-spectrometry: the AROMA setup. AROMA (Aromatic Research of Organics with Molecular Analyzer) is dedicated to the analysis, with micron-scale resolution, of the carbonaceous molecular content of cosmic dust analogues. The experimental setup consists of a microprobe laser desorption ionization chamber and a segmented linear quadrupole ion trap connected to an orthogonal time of flight mass spectrometer (LQIT-oTOF). For each detected m/z peak with a signal-to-noise ratio (S/N) greater than 10, a chemical formula was assigned using the mMass software⁵², an open source mass spectrometry tool. The double bond equivalent (DBE) for each molecular formula was then calculated using the following equation for a given chemical formula of hydrocarbon species C_cH_h : $DBE = c - (h/2) + 1$. This method allows sorting of the detected ions into families of compounds⁵³. This is done using empirical factors that delineate DBE boundaries in complex natural organic matter⁵⁴. Hydrocarbons with $0.5 < DBE/C < 0.9$ are considered to be aromatics. The line $DBE/C \sim 1$ corresponds to C clusters and the species falling in the zone $0.9 \leq DBE/C < 1$ are referred to as HC clusters, which includes C_cH_2 polyynes. Once all the detected species were sorted, the ion signal percentage was calculated for each family by dividing the sum of peak intensities detected in each family by the total ion intensity. The reported error bars in DBE analysis correspond to the relative standard deviation obtained for the total ion signal over a mass range of a family of compounds when the measurement was repeated several times (7 to 10) on natural samples. These error bars, of around 25%, are conservative since they have been derived from a complex matrix.

Thermal Programmed Desorption (TPD). Experiments were performed *in situ* to determine the mass spectra of the carbon analogues deposited on low reactivity surfaces annealed at increasing temperatures. TPD was performed using a Pfeiffer HiQuad QMG 700 with QMA 400 mass spectrometer with a CP 400 ion counter preamplifier. The instrumentation allows measurement of masses between 0 and 512 amu with a detection limit of 10^{-15} mbar. After carbon analogue deposition the samples were placed in front of the quadrupole at a short distance (>1 cm) ensuring that the majority of the collected gas species derive from the surface of the sample surface. Atomically flat Au(111) and HOPG substrates were used in the experiments, yielding comparable TPD spectra. Au(111) surfaces were cleaned *in situ* by the standard methodology of sputtering/annealing. HOPG was mechanically cleaved *ex situ* and consecutively introduced into the vacuum system, which ensures an atomically fresh graphite surface prior to deposition. The carbon analogues were deposited during 100 minutes, ensuring that there is sufficient carbon material to obtain well-defined signals in the TPD experiments. A temperature ramp of $12.5^\circ K \cdot min^{-1}$ was applied from room temperature to the maximum temperature examined (700K).

Acknowledgements. We thank the European Research Council for funding support under Synergy Grant ERC-2013-SyG, G.A. 610256 (NANOCOSMOS). Also, partial support from the Spanish Research Agency (AEI) through grants MAT2017-85089-c2-1R, FIS2016-77578-R and FIS2016-77726-C3-1-P is acknowledged. Support from the FotoArt-CM Project (P2018/NMT-

4367) through the Program of R&D activities between research groups in Technologies 2013, co-financed by European Structural Funds, is also recognised.

Author contributions. *In-situ* experiments in *Stardust* were performed by L.M, G.S, P.M, and M.Ac.; C.J. and H.S. performed LDI experiments. P.M.; K.L, R.O and A.M performed STM images. L.M. performed AFM images. R.J.P, V.J.H. and I.T. performed the OES experiments. M.Ag. made the kinetic calculations. G.J.E. and J.A.M-G wrote the first version of the manuscript. J.A.M-G supervised *in-situ* experiments, and C.J. and J.C the astrochemical interpretation. All authors discussed and contributed to the final version of the manuscript.

Data availability. The data that support the plots within this paper and other findings of this study are available from the corresponding author upon reasonable request.

Competing interests. The authors declare no competing interests.

Additional information. Additional text, figures and references are provided.

REFERENCES

1. Kwok, S. The synthesis of organic and inorganic compounds in evolved stars. *Nature* **430**, 985–991 (2004).
2. Henning, T. & Salama, F. Carbon in the universe. *Science* **282**, 2204–2210 (1998).
3. Meinert, C. *et al.* Ribose and related sugars from ultraviolet irradiation of interstellar ice analogs. *Science* **352**, 208–12 (2016).
4. Fonfria, J. P., Cernicharo, J., Richter, M. J. & Lacy, J. H. A Detailed Analysis of the Dust Formation Zone of IRC +10216 Derived from Mid-Infrared Bands of C₂H₂ and HCN. *Astrophys. J.* **673**, 445–469 (2008).
5. Cernicharo, J. *et al.* Infrared Space Observatory's Discovery of C₄H₂, C₆H₂, and Benzene in CRL 618. *Astrophys. J.* **546**, L123–L126 (2001).
6. Cami, J., Bernard-Salas, J., Peeters, E. & Malek, S. E. Detection of C₆₀ and C₇₀ in a young planetary nebula. *Science* **329**, 1180–2 (2010).
7. Gail, H., & Sedlmayr, E. (2013). *Physics and Chemistry of Circumstellar Dust Shells* (Cambridge Astrophysics). Cambridge: Cambridge University Press. doi:10.1017/CBO9780511985607
8. Schlemmer, S., Mutschke, H., Giesen, T. & Jäger, C. *Laboratory astrochemistry: From molecules through nanoparticles to grains*. (Wiley, 2014). doi:10.1002/9783527653133
9. Kroto, H. W., Heath, J. R., O'Brien, S. C., Curl, R. F. & Smalley, R. E. C₆₀: Buckminsterfullerene. *Nature* **318**, 162–163 (1985).
10. Jäger, C., Huisken, F., Mutschke, H., Jansa, I. L. & Henning, T. Formation of polycyclic aromatic hydrocarbons and carbonaceous solids in gas-phase condensation experiments. *Astrophys. J.* **696**, 706–712 (2009).
11. Biennier, L. *et al.* Characterization of circumstellar carbonaceous dust analogues produced by pyrolysis of acetylene in a porous graphite reactor. *Carbon N. Y.* **47**, 3295–3305 (2009).
12. Pino, T. *et al.* The 6.2 μm band position in laboratory and astrophysical spectra: a tracer of the aliphatic to aromatic evolution of interstellar carbonaceous dust. *Astron. Astrophys.* **490**, 665–672 (2008).
13. Contreras, C. S. & Salama, F. Laboratory investigations of polycyclic aromatic hydrocarbon formation and destruction in the circumstellar outflows of carbon stars. *Astrophys. Journal, Suppl. Ser.* **208**, (2013).
14. Peláez, R. J. *et al.* Plasma generation and processing of interstellar carbonaceous dust analogs. *Plasma Sources Sci. Technol.* **27**, 035007 (2018).
15. Fulvio, D., Gobi, S., Jaeger, C., Kereszturi, A. & Henning, T. Laboratory experiments on the low temperature formation of carbonaceous grains in the ISM. *Astrophys. J. Suppl. Ser.* **233**, 14 (2017).

16. Peeters, E., Spoon, H. W. W. & Tielens, A. G. G. M. PAHs as a tracer of star formation? *Astrophys. J.* **613**, 986–1003 (2004).
17. Sellgren, K. *et al.* C₆₀ IN REFLECTION NEBULAE. *Astrophys. J.* **722**, L54–L57 (2010).
18. García-Hernández, D. A. *et al.* FORMATION OF FULLERENES IN H-CONTAINING PLANETARY NEBULAE. *Astrophys. J. Lett.* **724**, 39–43 (2010).
19. Cordiner, M. A. *et al.* Confirming Interstellar C₆₀⁺ Using the *Hubble Space Telescope*. *Astrophys. J.* **875**, L28 (2019).
20. Kwok, S. & Zhang, Y. Mixed aromatic-aliphatic organic nanoparticles as carriers of unidentified infrared emission features. *Nature* **479**, 80–83 (2011).
21. Martínez, L. *et al.* Precisely controlled fabrication, manipulation and in-situ analysis of Cu based nanoparticles. *Sci. Rep.* **8**, 7250 (2018).
22. Frenklach, M. & Feigelson, E. D. Formation of polycyclic aromatic hydrocarbons in circumstellar envelopes. *Astrophys. J.* **341**, 372 (1989).
23. Ravagnan, L. *et al.* Cluster-Beam Deposition and in situ Characterization of Carbyne-Rich Carbon Films. *Phys. Rev. Lett.* **89**, 285506 (2002).
24. Haberland, H. in *Gas-Phase Synthesis of Nanoparticles* (ed. Huttel, Y.) 3–21 (Wiley-VCH, 2017). doi:10.1002/9783527698417
25. Lodders, K. & Fegley, B. Condensation Chemistry of Circumstellar Grains. *Symp. - Int. Astron. Union* **191**, 279–290 (1999).
26. Kratochvíl, J., Kuzminova, A., Kylián, O. & Biederman, H. Comparison of magnetron sputtering and gas aggregation nanoparticle source used for fabrication of silver nanoparticle films. *Surf. Coatings Technol.* **275**, 296–302 (2015).
27. Selwyn, G. S., Weiss, C. A., Sequeda, F. & Huang, C. Particle contamination formation in magnetron sputtering processes. *J. Vac. Sci. Technol. A Vacuum, Surfaces, Film.* **15**, 2023–2028 (1997).
28. Agúndez, M. *et al.* Molecular abundances in the inner layers of IRC +10216. *Astron. Astrophys.* **543**, A48 (2012).
29. Yang, X., Chen, P. & He, J. Molecular and dust features of 29 SiC carbon AGB stars. *Astron. Astrophys.* **414**, 1049–1063 (2004).
30. Bueno, R. A. *et al.* Highly selective covalent organic functionalization of epitaxial graphene. *Nat. Commun.* **8**, 15306 (2017).
31. Oyarzabal, E., Doerner, R. P., Shimada, M. & Tynan, G. R. Carbon atom and cluster sputtering under low-energy noble gas plasma bombardment. *J. Appl. Phys.* **104**, (2008).
32. Cernicharo, J. The Polymerization of Acetylene, Hydrogen Cyanide, and Carbon Chains in the Neutral Layers of Carbon-rich Proto-planetary Nebulae. *Astrophys. J. Lett.* **608**, L41 (2004).

33. Contreras, C. S., Sahai, R., de Paz, A. G. & Goodrich, R. Echelle long-slit optical spectroscopy of evolved stars. *Astrophys. J. Suppl. Ser. Vol. 179, Issue 1, pp. 166-194 (2008)*. **179**, 166–194 (2008).
34. Sabbah, H. *et al.* Identification of PAH Isomeric Structure in Cosmic Dust Analogs: The AROMA Setup. *Astrophys. J.* **843**, 34 (2017).
35. Van Orden, A. & Saykally, R. J. Small Carbon Clusters: Spectroscopy, Structure, and Energetics. *Chem. Rev.* **98**, 2313–2358 (1998).
36. Joblin, C., Leger, A. & Martin, P. Contribution of polycyclic aromatic hydrocarbon molecules to the interstellar extinction curve. *Astrophys. J.* **393**, L79 (1992).
37. Agúndez, M., Roueff, E., Le Petit, F. & Le Bourlot, J. The chemistry of disks around T Tauri and Herbig Ae/Be stars. *A&A* **616**, (2018).
38. Anichich, V. An index of the literature for bimolecular gas phase cation-molecule reaction kinetics. *JPL Publ. 03-19* 1172 (2003).
39. Clary, D. C. *et al.* C + C₂H₂: A Key Reaction in Interstellar Chemistry. *J. Phys. Chem. A* **106**, 5541–5552 (2002).
40. Pitts, W. M., Pasternack, L. & McDonald, J. R. Temperature dependence of the C₂(X¹Σ_g⁺) reaction with H₂ and CH₄ and C₂(X¹Σ_g⁺ and a 3Π_u equilibrated states) with O₂. *Chem. Phys.* **68**, 417–422 (1982).
41. Lodders, K. & Fegley, B. Condensation chemistry of carbon stars. in *Astrophysical implications of the laboratory study of presolar materials* **402**, 391–423 (ASCE, 1997).
42. Martin, P. G. & Rogers, C. Carbon grains in the envelope of IRC +10216. *Astrophys. J.* **322**, 374 (1987).
43. Atomic Spectra Database | NIST.
44. Alyabyev, S. B. & Beletskaya, I. P. Gold as a catalyst. Part II. Alkynes in the reactions of carbon–carbon bond formation. *Russ. Chem. Rev.* **87**, 984–1047 (2018).
45. Zaera, F. Surface chemistry of hydrocarbon fragments on transition metals: Towards understanding catalytic processes. *Catalysis Letters* **91**, 1–10 (2003).
46. Zhao, L. *et al.* Pyrene synthesis in circumstellar envelopes and its role in the formation of 2D nanostructures. *Nat. Astron.* **2**, 413–419 (2018).
47. Merino, P. *et al.* Graphene etching on SiC grains as a path to interstellar polycyclic aromatic hydrocarbons formation. *Nat. Commun.* **5**, 3054 (2014).
48. Tian, M. *et al.* Catalytic conversion of acetylene to polycyclic aromatic hydrocarbons over particles of pyroxene and alumina. *Philos. Trans. R. Soc. A Math. Phys. Eng. Sci.* **371**, (2013).
49. Cherchneff, I., Barker, J. R. & Tielens, A. G. G. M. Polycyclic aromatic hydrocarbon formation in carbon-rich stellar envelopes. *Astrophys. J.* **401**, 269 (1992).

50. Cherchneff, I. & Cau, P. The chemistry of carbon dust formation. *Symp. - Int. Astron. Union* **191**, 251–260 (1999).
51. Horcas, I. *et al.* WSXM: a software for scanning probe microscopy and a tool for nanotechnology. *Rev. Sci. Instrum.* **78**, 013705 (2007).
52. Strohalm, M., Kavan, D., Novák, P., Volný, M. & Havlíček, V. mMass 3: A Cross-Platform Software Environment for Precise Analysis of Mass Spectrometric Data. *Anal. Chem.* **82**, 4648–4651 (2010).
53. Marshall, A. G. & Rodgers, R. P. Petroleomics: Chemistry of the underworld. *Proc. Natl. Acad. Sci.* **105**, 18090–18095 (2008).
54. Koch, B. P. & Dittmar, T. From mass to structure: An aromaticity index for high-resolution mass data of natural organic matter. *Rapid Commun. Mass Spectrom.* **20**, 926–932 (2006).

Supplementary references, text and figures

Supplementary references

1. Martínez, L. *et al.* Precisely controlled fabrication, manipulation and in-situ analysis of Cu based nanoparticles. *Sci. Rep.* **8**, 7250 (2018).
2. Kroto, H. W., Heath, J. R., O'Brien, S. C., Curl, R. F. & Smalley, R. E. C₆₀: Buckminsterfullerene. *Nature* **318**, 162–163 (1985).
3. Jäger, C., Mutschke, H., Henning, T. & Huisken, F. Spectral Properties of Gas-phase Condensed Fullerene-like Carbon Nanoparticles from Far-ultraviolet to Infrared Wavelengths. *Astrophys. J.* **689**, 249–259 (2008).
4. Carpentier, Y. *et al.* Nanostructuring of carbonaceous dust as seen through the positions of the 6.2 and 7.7 μ m AIBs. *Astron. Astrophys.* **548**, A40 (2012).
5. Jäger, C. *et al.* Identification and Spectral Properties of Polycyclic Aromatic Hydrocarbons in Carbonaceous Soot Produced by Laser Pyrolysis. *Astrophys. J. Suppl. Ser.* **166**, 557–566 (2006).
6. Jäger, C., Huisken, F., Mutschke, H., Jansa, I. L. & Henning, T. Formation of polycyclic aromatic hydrocarbons and carbonaceous solids in gas-phase condensation experiments. *Astrophys. J.* **696**, 706–712 (2009).
7. Biennier, L. *et al.* Characterization of circumstellar carbonaceous dust analogues produced by pyrolysis of acetylene in a porous graphite reactor. *Carbon N. Y.* **47**, 3295–3305 (2009).
8. Kovačević, E., Stefanović, I., Berndt, J., Pendleton, Y. J. & Winter, J. A Candidate Analog for Carbonaceous Interstellar Dust: Formation by Reactive Plasma Polymerization. *Astrophys. J.* **623**, 242–251 (2005).
9. Contreras, C. S. & Salama, F. Laboratory investigations of polycyclic aromatic hydrocarbon formation and destruction in the circumstellar outflows of carbon stars. *Astrophys. Journal, Suppl. Ser.* **208**, (2013).
10. Maté, B., Molpeceres, G., Jiménez-Redondo, M., Tanarro, I. & Herrero, V. J. High-energy electron irradiation of interstellar carbonaceous dust analogs: cosmic-ray effects on the carriers of the 3.4 μ m absorption band. *Astrophys. J.* **831**, 51 (2016).
11. Agúndez, M. *et al.* Molecular abundances in the inner layers of IRC +10216. *Astron. Astrophys.* **543**, A48 (2012).
12. Fonfría, J. P. *et al.* The Abundance of C₂H₄ in the Circumstellar Envelope of IRC+10216. *Astrophys. J.* **835**, 196 (2017).
13. Haberland, H. in *Gas-Phase Synthesis of Nanoparticles* (ed. Huttel, Y.) 3–21 (Wiley-VCH, 2017). doi:10.1002/9783527698417
14. Agúndez, M. *et al.* Growth of carbon chains in IRC +10216 mapped with ALMA***. *A&A* **601**, (2017).
15. Gail, H., & Sedlmayr, E. (2013). *Physics and Chemistry of Circumstellar Dust Shells* (Cambridge Astrophysics). Cambridge: Cambridge University Press. doi:10.1017/CBO9780511985607

16. Kousal, J. *et al.* Magnetron-sputtered copper nanoparticles: lost in gas aggregation and found by in situ X-ray scattering. *Nanoscale* **10**, 18275–18281 (2018).
17. Kwok, S. The synthesis of organic and inorganic compounds in evolved stars. *Nature* **430**, 985–991 (2004).
18. Kratochvíl, J., Kuzminova, A., Kylián, O. & Biederman, H. Comparison of magnetron sputtering and gas aggregation nanoparticle source used for fabrication of silver nanoparticle films. *Surf. Coatings Technol.* **275**, 296–302 (2015).
19. Haberland, H., Karrais, M. & Mall, M. A new type of cluster and cluster ion source. *Zeitschrift für Phys. D Atoms, Mol. Clust* **415**, 413–415 (1991).
20. Michau, A., Arnas, C., Lombardi, G., Bonnin, X. & Hassouni, K. Nanoparticle formation and dusty plasma effects in DC sputtering discharge with graphite cathode. *Plasma Sources Sci. Technol.* **25**, (2016).
21. De Toro, J. A., Normile, P. S. & Binns, C. in *Gas-Phase Synthesis of Nanoparticles* 39–55 (2017).
22. Binns, C. in *Handbook of Metal Physics* 49–71 (2009).
23. Selwyn, G. S., Weiss, C. A., Sequeda, F. & Huang, C. Particle contamination formation in magnetron sputtering processes. *J. Vac. Sci. Technol. A Vacuum, Surfaces, Film.* **15**, 2023–2028 (1997).
24. Sabbah, H. *et al.* Identification of PAH Isomeric Structure in Cosmic Dust Analogs: The AROMA Setup. *Astrophys. J.* **843**, 34 (2017).
25. Šedo, O., Alberti, M., Janča, J. & Havel, J. Laser desorption-ionization time of flight mass spectrometry of various carbon materials. *Carbon N. Y.* **44**, 840–847 (2006).
26. Horný, L., Petraco, N. D. K. & Schaefer, H. F. Odd carbon long linear chains HC_{2n+1}H (n = 4–11): Properties of the neutrals and radical anions. *J. Am. Chem. Soc.* **124**, 14716–14720 (2002).
27. Maclagan, R. G. A. R. The proton affinity of C₃H₂. *J. Mol. Struct. THEOCHEM* **258**, 175–178 (1992).
28. Sánchez, J. P., Aguirre, N. F., Díaz-Tendero, S., Martín, F. & Alcamí, M. Structure, Ionization, and Fragmentation of Neutral and Positively Charged Hydrogenated Carbon Clusters: C_nH_m^{q+} (n = 1–5, m = 1–4, q = 0–3). *J. Phys. Chem. A* **120**, 588–605 (2016).
29. Cordiner, M. A., Charnley, S. B., Kisiel, Z., McGuire, B. A. & Kuan, Y.-J. Deep K-band observations of TMC-1 with the Green Bank Telescope: Detection of HC₇O, non-detection of HC₁₁N, and a search for new organic molecules. *Astrophys. J.* **850**, 187 (2017).
30. McGuire, B. A. *et al.* Detection of Interstellar HC₅O in TMC-1 with the Green Bank Telescope. *Astrophys. J.* **843**, L28 (2017).
31. A. Pinaridi *et al.* Tailored formation of N-doped nanoarchitectures by diffusion-controlled on-surface (cyclo) dehydrogenation of heteroaromatics. *ACS nano* **7**, 3676–3684 (2013)

1. The stardust machine and the CSE: Technical details.

The Stardust machine for mimicking the CircumStellar Envelope (CSE)

The Stardust machine is a novel experimental setup designed to simulate in the laboratory the complex conditions of cosmic dust formation and processing in the environment of evolved stars or supernova. It comprises six interconnected ultra-high-vacuum (UHV) modules, offering a high level of control over both the fabrication and processing of cosmic dust analogues. In addition, a collection of *in situ* characterization techniques is available. In *Stardust* the chemistry proceeds via atom aggregation under conditions in which most of the reactions that occur are neutral-neutral, closely resembling what happens in the circumstellar envelopes (CSE) of Asymptotic Giant Branch (AGB) stars.

The *Stardust* machine was conceived as a multi-purpose experimental station. Thus, it has a versatile, modular design that allows easy reconfiguration of the machine based on the requirements of each specific experiment. Each module has been designed to simulate a given process in a given astrophysical environment. The first step corresponds to the generation of dust seeds, which can be produced at relatively low temperature in the first module, denominated *Multiple Ion Cluster Source (MICS)*, where atoms are ejected from up to three targets. During their transit along this module atoms start to aggregate through collisions with other ejected atoms and the growth process occurs. After production, the seeds pass through a *Diagnosis chamber*, where it is possible to monitor, filter and perform experiments on these pristinely formed seeds. Subsequently, the seeds enter the *Oven chamber*, a passageway where the seeds can be heated with IR radiation during their transit. This can provide temperatures similar to those found in the dust formation zone of AGBs. Upon exiting the *Oven chamber* the grains can be accelerated in the *Acceleration module*, in order to simulate radiation pressure or the escape of the grains towards the interstellar medium (ISM), where the material will cool down. Furthermore, gas phase molecules (H_2 , CH_4 , C_2H_2 ...) can be introduced into any of the previously described chambers in desired proportions, in order to promote gas-grain interactions.

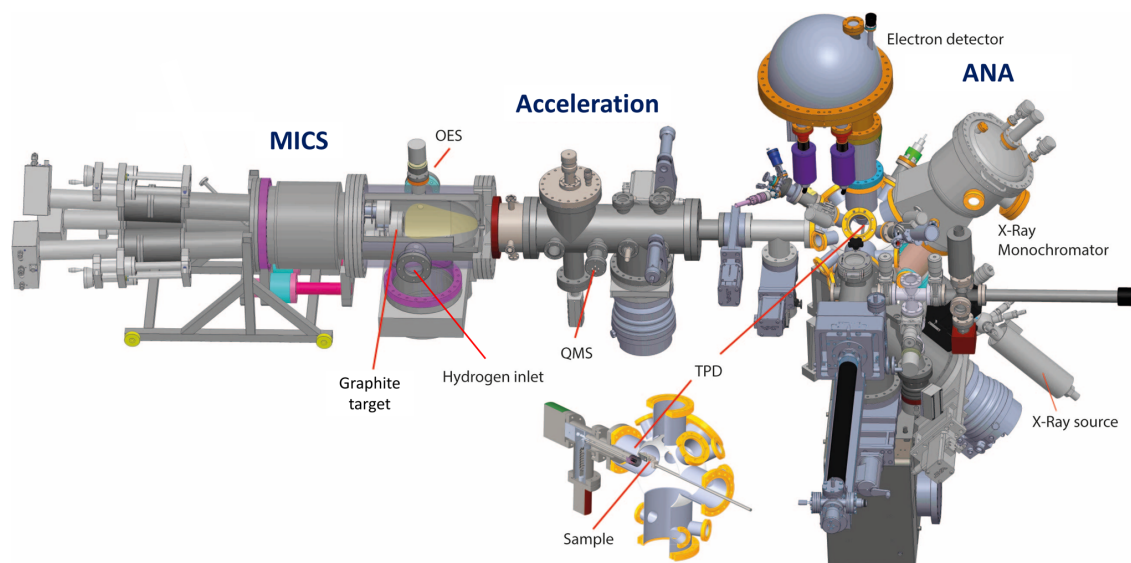
After the fabrication of the dust analogues, the next modules are dedicated to both analysing the properties of the generated pristine analogues, as well as tackling the question of dust evolution in various astrophysical environments ranging from later stages of evolved stars (protoplanetary and planetary nebulae), to the ISM and protoplanetary disks. The *INFRA-ICE module* is dedicated to performing IR spectroscopy of analogues formed at variable temperature down to 12 K, allowing on-substrate (by collecting the analogues) dust processing and molecular ice growth. The final module is the *ANA (Analysis Module)* that consists of a UHV chamber in which the dust analogues are collected on a substrate and further analysed by a collection of surface science techniques (XPS, Auger, UPS, LEIS...). Here the collected analogues can be heated to up to 1200 K combined with various dust processing techniques. All the processes occurring to the dust analogues during heating, irradiation and exposure can be monitored *in situ* by the available characterization techniques.

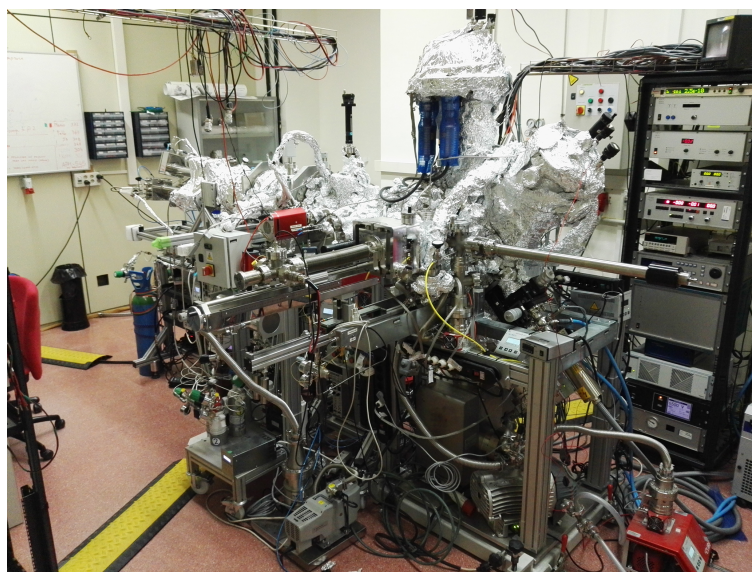
A detailed technical description of the overall machine is provided in reference¹. The experiments presented in this article correspond to a short configuration of the machine, in which only some of the modules have been used. Given the aforementioned need for highly

controllable and clean environments to undertake proper laboratory simulations, only ultra-high vacuum (UHV) compatible materials and seals were used in the construction of the machine.

Configuration of the Stardust set-up used in present experiments

Although the modular concept of the Stardust machine allows to be mounted in different configurations, for this work only three chambers were employed: MICS, Acceleration and ANA. The MICS module is a sputter gas aggregation source (SGAS) devoted to nanoparticle (NP) and cluster fabrication. It incorporates lateral entrances in the aggregation zone through which both Optical Emission Spectroscopy (OES) and gas (H_2) injection is performed. The Acceleration module in this configuration is dedicated to monitor the NPs. In this work it was employed for sample collection for *ex situ* analysis and for Quadrupole Mass Spectrometry (QMS). Finally, the ANA module is devoted to *in situ* analysis of the NPs by electron spectroscopy techniques and thermal desorption spectroscopy. Further details of each module are given elsewhere¹. Supplementary Figure 1 shows the configuration employed in this work. For the collection of the carbon star-dust analogues, two different fast entry points were used (in the Acceleration and ANA chambers). Unless otherwise specified, the samples were collected in the *Acceleration chamber*. The base pressure was 1×10^{-9} in MICS, 5×10^{-10} in Acceleration, and 1×10^{-10} mbar in ANA.





Supplementary Figure 1. Technical drawing (top) and photograph (bottom) of *Stardust* in the configuration employed for these experiments.

2.- Comparison between *Stardust* and other methods for fabricating carbon star-dust analogues.

Several methodologies for generating carbon star-dust analogues have been proposed in the literature resulting in a number of carbon products with different structure and hydrogen content. The main production techniques are summarized in Supplementary Table 1. This table collects the main physical parameters. Some of the parameters cannot be easily generalized as they are strongly dependent on the experimental conditions. This is the case of the total pressure, where a great deal of precision is needed to define this value (base pressure, pressure of the dragging or residual gas, partial pressure of the precursors, etc.). The list of references is representative and far from being exhaustive, as there are many of insightful experiments that have been performed in laboratory astrophysics.

Supplementary table 1: Comparison between typical techniques used to synthesize cosmic dust analogues.

Technique	Precursors	T (K)	Ion chemistry	Wall effect	Refs
Laser ablation	Graphite + quenching gas	≥ 4000	yes	no	2,3
Combustion/Flames	Hydrocarbons	1800-2500	weak	no	4
Pyrolysis (laser induced)	Hydrocarbons	1000-1700 ≥ 3500	no	depending on reactor	5,6
Pyrolysis	Hydrocarbons	600-2000	no	depending on reactor	7
Dusty plasmas	Hydrocarbons	600-2000	Weak/	yes	8-10

SGAS: Sputter Gas aggregation sources: <i>Stardust</i>	Graphite + H ₂	<1000	strong weak/no	no	This work
--	---------------------------	-------	-------------------	----	-----------

All the aforementioned techniques have been used to describe different conditions and regions of the cosmos. However, they present limitations as the experiments used to mimic astrophysical environments need to be scaled to laboratory standards, and on many occasions, it is very difficult to validate a technical set-up as representative of particular astronomical conditions. This is mostly true when trying to reproduce the chemistry of the inner layers of CSE of evolved stars. In most of these experiments the chemistry involves high-energetic or ionic content, out of equilibrium processes, or relies on molecular precursors that must be decomposed. These conditions are far removed from those of the inner layers of CSE, where clustering takes place mostly by neutral-neutral reactions in the absence of other sources of radiation. In this respect, the *Stardust* machine was specifically conceived for reproducing the inner layers of the CSE, and its differential advantage with respect to the rest of the dust analogue production techniques is that the basic constituents from which the material grows are individual thermalized atoms. This is critical in all the three steps of the dust growth process and enables us to obtain chemical synthesis routes from reactions in equilibrium, as observed in C-rich AGB stars and some protoplanetary nebulae.

Supplementary table 2. Table comparing the dust formation zone of CSEs with the experimental values used for experiments in *Stardust*.

Typical values in the dust formation zone of CSEs	Values at aggregation zone of <i>Stardust</i>	Comments
$n_{\text{H}_2} = 10^8 - 10^{12} \text{ cm}^{-3}$. Ref ¹¹ $n_{\text{H}_2}/n_{\text{C}} = 10^3$	$n_{\text{H}_2} = 10^{10} - 10^{12} \text{ cm}^{-3}$ $n_{\text{H}_2}/n_{\text{C}} = 1 - 10^2$	<i>Stardust</i> densities are higher to accelerate the chemistry. The high end of the H ₂ /C ratio is close to that of the CSE.
Temperature range: 500-2000 K. Ref ^{11,12}	Temperature range: 300-500K	The chemical kinetics model suggests that the effect of temperature is critical for the formation of alkanes, which are favored at low temperatures. Close to the magnetron surface, temperature can reach around 1000K, although at the aggregation area could be below 500K. ¹³
Absence of UV processing. Ref ¹⁴	Absence of UV photons.	Possible UV photons from the UV interstellar field in low mass loss rate AGB stars or in very clumpy envelopes
Ionization degree: <10 ⁻⁵ . Ref ¹⁵	Ionization degree: 10 ⁻⁵ . Ref. ¹³	The charge is found mainly on large particles after they are formed. Not playing important role in the chemistry of small molecules and clusters.

$n_{\text{H}_2}/n_{\text{C}_2\text{H}_2}$: Estimated: 10^4 Ref. ¹⁴ Detected: 10^7 Ref. ¹⁶	Acetylene is produced, not introduced : $n_{\text{H}_2}/n_{\text{C}_2\text{H}_2}$: 50	We produce an excess of C_2H_2 with respect to the star, however, still low enough to initiate cyclization in these conditions
Time in this area: 30 yr, to travel 10^{15} cm at a expansion velocity of 10 km/s. · Ref ¹¹	Residence time in aggregation zones: seconds: Ref. ¹⁶	In Stardust the Ar pressure close to the magnetron enables 3-body reactions
Gas phase aggregation from atoms	Gas phase aggregation from atoms	Not necessary to include molecular precursors to decompose as source of C or highly energetic plasma to initiate the chemistry
Shock waves. · Ref ¹⁷	No shocks	Material formed in shocks cannot be simulated in <i>Stardust</i>

Sputter gas aggregation sources (SGAS) compared to Magnetron sputtering. Gas phase condensation techniques have been widely reported as good candidates for the formation of cosmic dust grain analogues⁶. Traditionally, in gas aggregation sources (GAS) atoms are evaporated to a region containing a cooling working gas. Upon reaching supersaturation and due to the collisions with the cooling gas, the atoms may nucleate to nanoparticles. These nanoparticles are afterwards dragged through a nozzle into another chamber with lower pressure, usually employed for deposition of the nanoparticle beam on a substrate¹⁸. Haberland and co-workers¹⁹ combined this idea of the GAS with magnetron sputtering and developed the so-called SGAS. The SGAS have some characteristics that clearly differentiate the technique from sputtering techniques commonly used for the creation of dusty plasmas²⁰. Biederman's group published a comparative study between both techniques¹⁸. One of the critical questions is the possibility of working at higher pressures of the working gas. Conventional sputtering processes usually operate in the $10^{-2} - 10^{-3}$ mbar range, while the pressure in the aggregation zone of a SGAS is in the range of 0.1-1 mbar²¹. In these conditions, clustering is highly efficient as the sputtered vapour is rich in dimers (formed by condensation of atoms and not directedly sputtered out from the target), which helps to overcome the energy barriers involved in the first stages of cluster nucleation, as this is considered to be a critical bottleneck in the clustering process²².

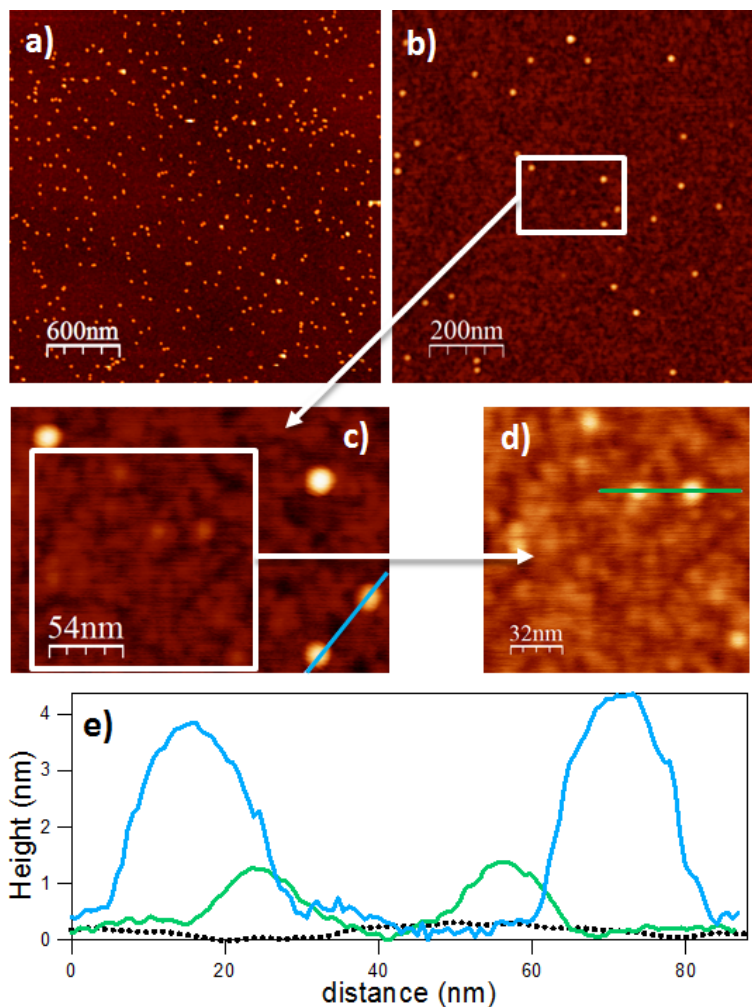
In SGAS, one chamber is used for sputtering and cluster growth and, subsequently, the nanoparticles are dragged by pressure difference into a secondary deposition chamber where the substrate is located. The SGAS process is not substrate dependent such that the nanoparticles, already formed in the first chamber, soft-land on the substrate instead of growing on the substrate as in conventional sputtering. Although the growth rates in SGAS are much slower than the sputtering processes (sputtering machines are designed to grow thick layers of a material on a substrate, whereas we focus on the first formed particles), the possibility to tune

the size (typically 1-60 nm)²¹ and the amount of nanoparticles generated with the variables of the process clearly represents an advantage in comparison to conventional sputtering, since lateral growth due to surface diffusion processes²³ is avoided.

Thus, in this article we propose the use of SGAS as a valuable and versatile technique for mimicking the conditions of CSE.

3. Atomic Force Microscope imaging (AFM).

AFM images were acquired *ex situ*, after fabrication of the samples using the fast entry point in the Acceleration chamber, marked as SAMPLE 1 position in Fig.1 of the main text. Supplementary Figure 2a corresponds to a deposition carried out during 10 min under the conditions described in the main text, whereby a nanoparticle rate of $8 \text{ NPs}/\mu\text{m}^2\cdot\text{min}$ can be derived. Most of the carbon is agglomerated in the form of nanometer size C-nanograins, as those that can be observed. Also, the substrate presents certain unresolved roughness comprised of smaller structures that may be related to the C/HC clusters detected with AROMA (white square in supplementary figure 2c). The features of the background and the C-nanograins can be easily differentiated from the line profiles. It is clear that on one hand there are C-nanograins of around 4 nm height (blue profile) and, even though they cannot be fully resolved using AFM, the structures depicted in the green profile present a height of around 1 nm. The former may be related to the structures presented in the STM analysis of Figure 2 in the main manuscript. The roughness of these small features is clearly larger than the roughness of the SiOx substrate (dashed-black line).

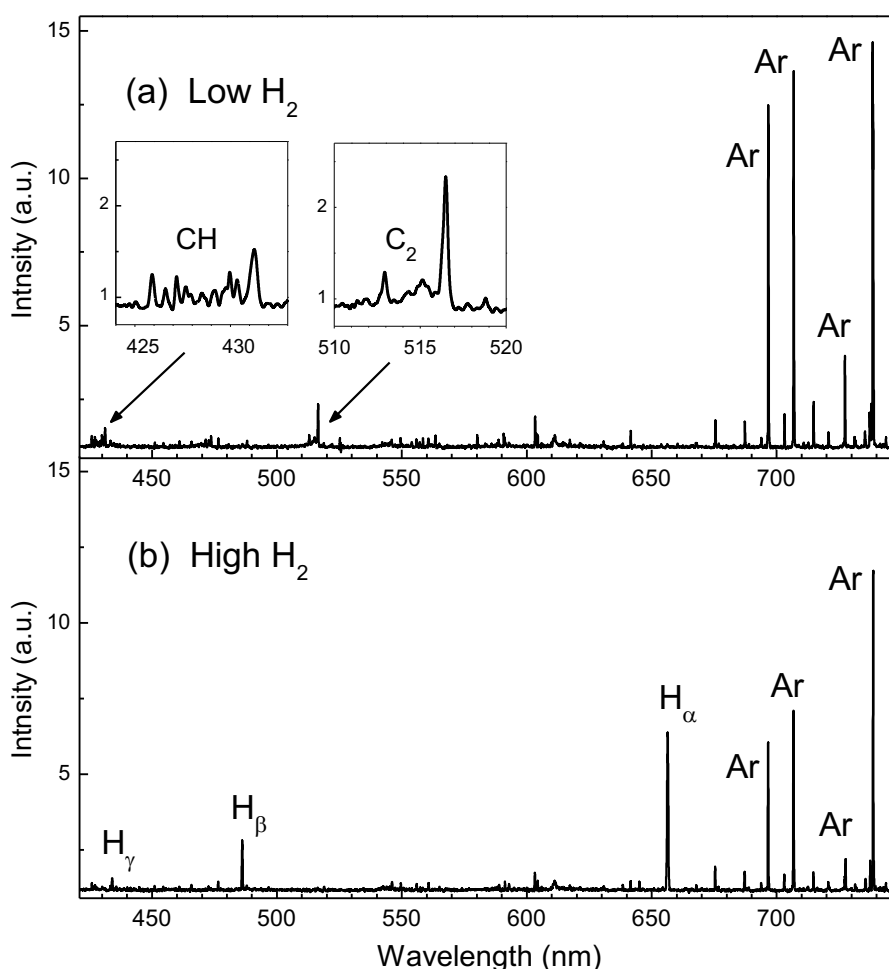


Supplementary Figure 2. AFM images of C-nanograins deposited on SiOx acquired at different magnifications. a) Image of $3 \mu\text{m} \times 3 \mu\text{m}$ indicating the size homogeneity of the nanograins. b) Image of $1 \mu\text{m} \times 1 \mu\text{m}$ of C-nanograins fabricated with half of the power employed for a) to have lower nanograin

density and smaller features on the surface. c) Zoom of figure b). d) Zoom of figure c). e) Height Profiles obtained from the blue and green lines of c) and d), respectively, compared to the height profile in a SiO_x substrate (dashed-black line). These images were recorded for a low hydrogen density.

4.- *In situ* optical emission spectroscopy

The emission spectra recorded during the production of carbon dust analogs in the aggregation zone of the stardust at different H₂ densities show that near infrared Ar lines prevailed in all cases, as shown in Supplementary Figure 3 for the 690 - 750 nm range. They correspond mainly to electronic transitions between the 4p-4s excited Ar levels, and extend up to 1000 nm. On the contrary, Ar emissions in the region 350-470 nm, corresponding to transitions 5p-4s that are usually very intense, have not been detected, due to the higher electron energy necessary to excite the upper level and to the fact that low Ar excitation temperatures (<1 eV) have been reported previously for this experimental system¹. Furthermore, C₂ and CH could be detected with low H₂ densities (see insets in Supplementary Fig. 4 (a)), but these bands disappeared when a high H₂ density was added. At the same time, Ar intensities decreased noticeably with increasing H₂, while the (H_α, H_β, H_γ) atomic lines of the Balmer series appeared.

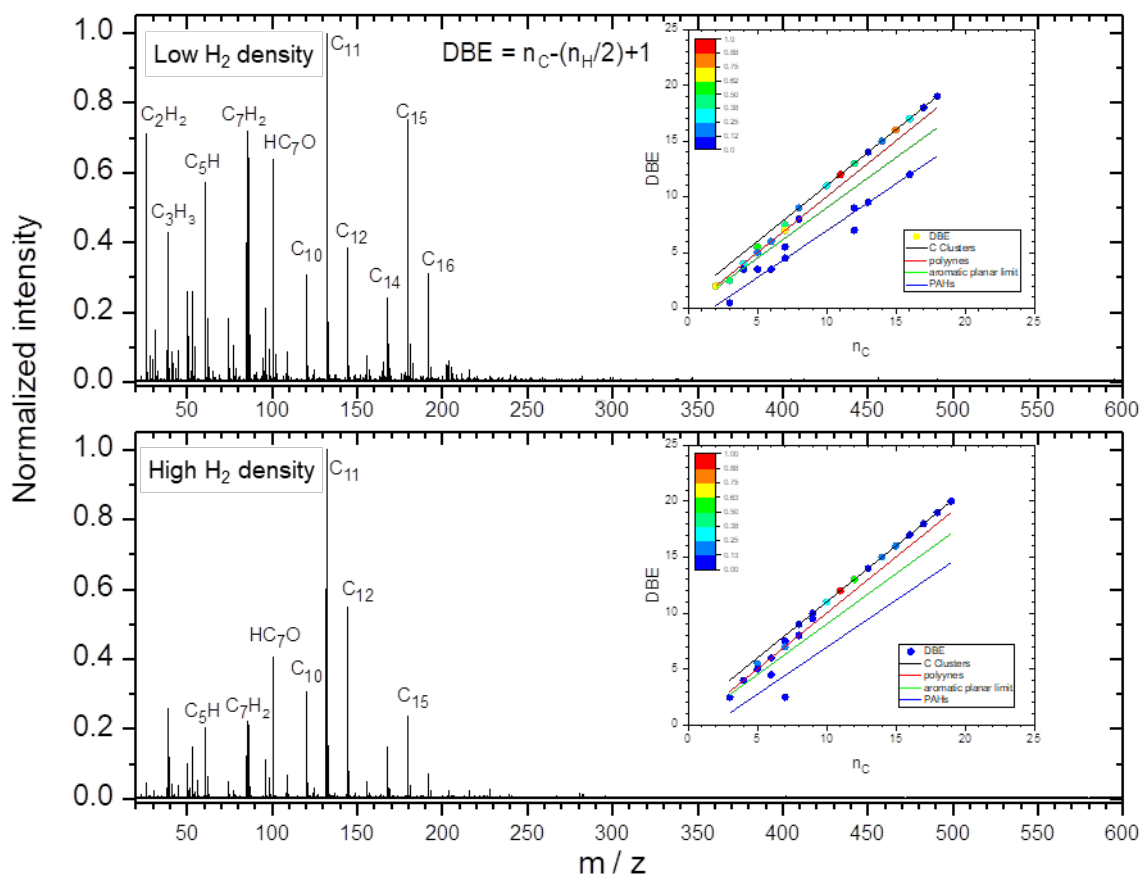


Supplementary Figure 3. Optical emission spectrum of the plasma generated in the aggregation zone of *Stardust* for a low (a) and a high (b) H₂ density. H₂ flow rates of 4x10⁻⁴ and 1 sccm were used, respectively.

5. Laser Desorption/Ionization (LDI) mass-spectrometry: the *AROMA* set-up

In order to obtain better insight into the molecular phase associated with the C-dust we have employed *ex situ* laser desorption ionization mass-spectrometry (LDI-MS) in the experimental set-up called *AROMA*²⁴. The ion source offers the possibility of probing polycyclic aromatic hydrocarbons (PAHs), carbon clusters (C clusters), hydrogenated carbon clusters (HC clusters) and fullerenes in solid samples by performing LDI in a single step²⁵ as well as using the laser desorption-laser ionization (L2MS) technique²⁴, in which desorption and ionization are separated in time and space and each step is performed with a different laser. In the L2MS scheme, the approach used in these experiments, an infrared laser pulse desorbs the solid material into the gas phase, with minimal fragmentation, and a subsequent ultraviolet (UV) laser pulse selectively ionizes the gas phase aromatic organic molecules. The ions generated are stored and thermalized in the linear quadrupole ion trap (LQIT) and then monitored with Time Of Flight (TOF) spectrometry. This technique has many advantages including its sensitivity. However, one drawback is that it is biased towards species that efficiently respond to the excitation scheme, in particular regarding ionization. For example, with the lasers used in our experiments, it is not possible to detect alkanes. On the other hand, the scheme is very sensitive to the detection of PAHs and fullerenes²⁴.

Supplementary Fig. 4 presents the full range mass spectra obtained with *AROMA*. $C_nH_2^+$ species are observed together with C_nH^+ species only for odd n values. The neutral precursors are expected to be C_nH_2 . For even n , polyynes are the expected structure. For odd n , the situation is more complicated with a competition between cumulenic and polyacetylenic structures²⁶, which most likely accounts for the fact that we observe both C_nH^+ and $C_nH_2^+$ species. Regarding smaller species, detection of $C_2H_2^+$ and $C_3H_3^+$ are notable. Both species are believed to be produced during the LDI analysis from the common C_3H_2 precursor. Indeed the latter species has a very high proton affinity²⁷. In addition, a major dissociation channel of $C_3H_2^+$ leads to $C_2H_2^+ + C$ ²⁸, which is a favourable production mechanism for $C_2H_2^+$ in the *AROMA* conditions, whereas direct ionization of C_2H_2 is not a viable mechanism. Finally, evidence for oxidation was seen with a major peak corresponding to HC_7O and a weak one that could be attributed to HC_5O . It should be noted that these two stable species nor any other HC_nO species have been detected in the ISM^{29,30}. These were the only oxidized species that were detected and it is likely that they were formed by reaction of the deposited molecular precursors with environmental oxygen.

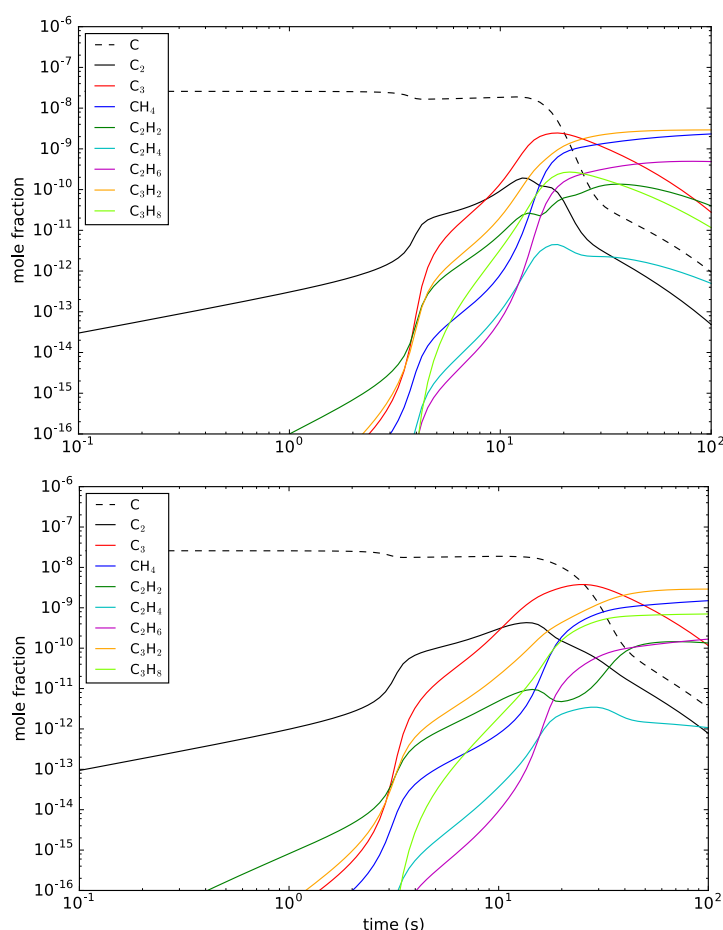


Supplementary Figure 4. Full range mass spectra obtained with *AROMA* for *Stardust* samples at low and high H₂ densities. The mass peaks are assigned to a chemical formula corresponding to neutral species. Although the laser technique used in *AROMA* minimizes fragmentation compared, for instance, to electron bombardment in a QMS, one should note that fragments of the neutral precursors can be present. Mass peaks corresponding to C clusters and HC clusters were found to dominate the spectra. The distributions of chemical species sizes span from 2 carbon atoms (C₂H₂) to a maximum of 19 carbon atoms (C₁₉) with the highest peak corresponding to C₁₁. The inventory of chemical species looks very similar in both cases, with some variations in the relative peak intensities. The DBE vs carbon number representation (see insets) provides a clearer view of the families of compounds dominating the mass spectra.

The apparent trend of a larger abundance of C clusters relative to HC clusters with the H₂ dose must be treated with caution, considering the error-bars. The reported error bars correspond to the relative standard deviation obtained for the total ion signal over a mass range of a family of compounds when the measurement was repeated several times (7 to 10) on natural samples. These error bars, of around 25%, are conservative since they have been derived from a complex matrix.

6.- Effect of the temperature in the kinetics models

Apart from the calculations presented in the main text carried out at 500 K, we have performed calculations at other temperatures to evaluate the sensitivity of the calculated abundances to the temperature. We have changed the pressure to use the same density of particles in all calculations and evaluate exclusively the influence of temperature. Supplementary Fig 6 presents an example. At lower temperatures (300 K) the results are qualitatively similar to those obtained at 500 K, with small variation in the peak abundances within the decade. Some masses are slightly higher whereas other decrease. These slight abundance deviations are caused by the dependence of the rate coefficients of the involved reactions in the molecular synthesis. At temperatures higher than 500 K the results gradually modify their trend, with unsaturated hydrocarbons like polyacetylenic chains becoming more abundant at the expense of saturated hydrocarbons, like alkanes. At temperatures above 1000 K the model predicts that the abundance of alkanes should be negligible.

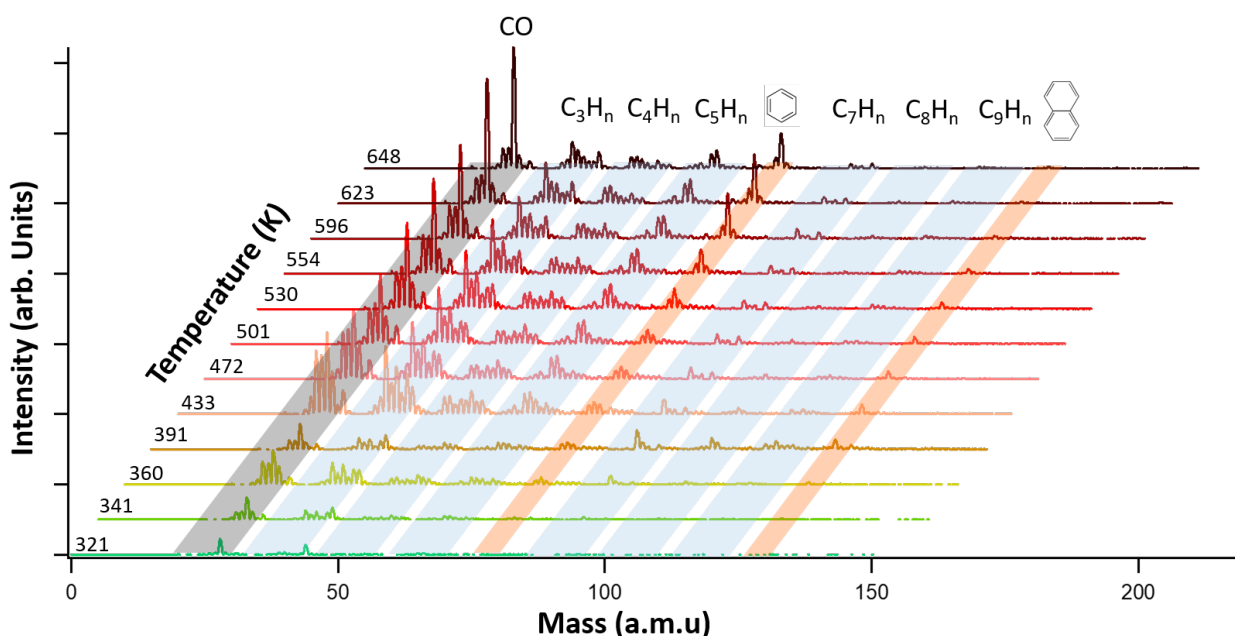


Supplementary Figure 5. Computed kinetic evolution of the formed species at different temperatures. Evolution of the chemical composition computed with the chemical kinetics model as the gas flows in the aggregation zone at 500K (upper figure) and 300K (lower figure).

7. Thermal Programmed Desorption

In Supplementary Fig. 6 we show a representative TPD experiment. The carbon analogues are deposited in ANA module on a Au(111) surface and annealed *in situ* at increasing temperatures. Mass spectrometry is recorded while increasing the temperature. As commented in the main text, consecutive families of small hydrocarbons with increasing carbon number of the family type C_kH_n , with $1 < k < 9$ are identified at increasing temperatures (highlighted with blue background). The small hydrocarbons start to desorb from the surface at temperatures as low as 340 K. At higher temperatures, the desorption of small hydrocarbons has occurred and the intensity of the peaks of the associated compounds decreases compared with those obtained at lower temperatures. A good example can be seen in the family C_3H_n which reaches its maximum intensity at a temperature of 433K. At higher temperatures benzene and naphthalene begin to be detected (highlighted with red background).

Importantly the intensity of the associated peak at 78 a.m.u increases with temperature. The increase is monotonous up to the maximum temperature examined of 700K. We also can distinguish mass 91, which can be attributed to toluene fragmentation. These results point towards the processing-induced formation of benzene after thermal processing of the analogues that is possibly mediated by the catalytic activity of the surface. However, we must point out that Au surfaces are notorious for their low-reactivity and low catalytic activity³¹. We have obtained similar results for TPD experiments on other inert substrates such as HOPG and SiOx. Therefore, aromatic formation from thermal processing of the analogues seems to be a robust process. In the real environment of AGB stars other processing mechanisms apart from temperature may be present, such as UV absorption or ionization radiation, which may further promote the conversion of non-aromatics into aromatic molecules and suggest an alternative route for the formation of PAHs.



Supplementary Figure 6. Thermal programmed desorption of the carbon analogues formed with high hydrogen density deposited on Au(111) annealed at increasing temperatures The temperature at the start

of each spectrum is marked on the left-hand side of the figure.. Spectral range from 20 to 150 a.m.u. The spectra are vertically shifted for clarity.